Iranian Journal of Fuzzy Systems

Volume 22, Number 5, (2025), pp. 1-19

Original paper

University of Sistan and Baluchestan

Improving quadrotor trajectory tracking by replacing PD critics with fuzzy critics in an adaptive critic-based neurofuzzy controller

A. R. Pourmoayed [1], M. A. Ranjbar [2] and M. A. Heidarpour [3]

[1,2] *Mechanical Engineering Department, Khatam Al-Anbia Air Defense University, Tehran, Iran.*
[3] *Mechanical Engineering Department, Amirkabir University of Technology, Tehran, Iran.*

a.pourmoayed@khadu.ac.ir, m.ranjbar@khadu.ac.ir, aliheidar@aut.ac.ir

Abstract

Quadrotors are increasingly employed in a wide range of applications, including surveying, agriculture, military operations, and rescue missions, due to their superior maneuverability. However, achieving accurate and stable control continues to pose a significant challenge. This study aims to enhance the performance of an adaptive critic-based neurofuzzy controller for quadrotors by replacing the conventional proportional-derivative (PD) critics with fuzzy critics. The control performance was quantitatively evaluated using the root mean square error (RMSE) criterion. Simulation results demonstrate that incorporating fuzzy critics improves performance by more than 39% compared to the traditional PD-based approach. To evaluate the trajectory tracking performance of the adaptive fuzzy-critic-based neurofuzzy controller under disturbance, external disturbances were introduced into the quadrotor model. The controller employing fuzzy critics exhibited strong disturbance rejection, maintaining accurate trajectory tracking despite external interferences. These findings highlight the effectiveness of fuzzy-critic-based neurofuzzy controllers in improving quadrotor trajectory tracking performance under dynamic and uncertain real-world conditions.

Keywords: Adaptive critic-based neurofuzzy controller, fuzzy critic, PD critic, quadrotor.

1 Introduction

Quadrotors have garnered significant attention from researchers due to their extensive applications in diverse fields, including surveying [5], agriculture [32], surveillance [7], and wildlife monitoring [26], as well as their advantages over other types of unmanned aerial vehicles (UAVs) [4].

Various control strategies have been employed to regulate quadrotors. Among these, linear control methods such as the proportional-integral-derivative (PID) controller [20] and the linear quadratic regulator (LQR) [35] are commonly used. However, due to the poor performance of these controllers under disturbances and when operating far from equilibrium, several studies have sought to enhance their effectiveness by integrating them with other techniques. For instance, some approaches involve using a fuzzy logic system to adjust the PID coefficients dynamically or employing a genetic algorithm to optimize the LQR weight matrices [6, 13, 17, 19, 21, 25, 30, 31, 34].

Nonlinear control methods represent another class of control strategies applied to quadrotors. Notable examples of these methods include the backstepping approach [9, 16], feedback linearization [27], and sliding mode control [2, 12, 14, 15, 22].

Nonlinear controllers typically require precise tuning of coefficients and possess complex structures. In contrast, artificial intelligence (AI)-based control methods have significantly reduced these challenges while maintaining effective disturbance rejection. Notable AI-based strategies for quadrotor control include fuzzy logic controllers [8, 15, 18] and machine learning-based controllers [1, 29]. Another category of AI-based controllers is the brain emotional learning-based intelligent controller (BELBIC), initially introduced for quadrotor control in [11].

Corresponding Author: M. A. Heidarpour
Received: April 2025; Revised: August 2025; Accepted: September 2025.
https://doi.org/10.22111/ijfs.2025.51627.9127

Although the BELBIC demonstrates strong learning capabilities, a model-free structure, and effective disturbance handling, it is more sensitive to parameter variations than other AI-based controllers such as the adaptive critic-based neurofuzzy controller (ACNFC). The ACNFC has been applied in various domains, including vehicle suspension vibration control [36], unmanned bicycle control [33], milling system control [3], and quadrotor control [28].

Recent research in fuzzy and learning control supports and strengthens the foundations of our proposed ACNFC-based quadrotor tracking system. The study [24] develops a model-free, data-driven approach to adjust fuzzy controller parameters using closed-loop experiments, backed by rigorous stability analysis via Popov's hyperstability theory—an approach conceptually akin to our adaptive fuzzy critic, which also refines control policies through feedback-driven learning. The article [10] presents a two-tiered framework, where a global planner is complemented by a local fuzzy controller that adeptly manages dynamic obstacles—demonstrating how fuzzy inference can effectively navigate real-time nonlinearities, much like our fuzzy critic handles aerial uncertainties. Finally, the study [37] applies a cascade of Lyapunov, sliding mode, and PID controllers to manage a highly nonlinear electromagnetic suspension, ensuring robust stability—mirroring our quadrotor system, where hybrid intelligent structures and cascade reasoning underpin robust trajectory tracking under disturbances. Collectively, these studies illustrate the adaptability, stability, and resilience of fuzzy and cascade learning-based control architectures—qualities that our ACNFC framework extends into the domain of aerial robotics.

Moreover, recent advances in fuzzy-control research underscore the critical importance of rigorous stability analysis for adaptive systems. The study [23] offers a comprehensive survey of fuzzy controllers applied in mechatronics—covering Takagi–Sugeno (TS) model-based, data-driven, and evolving systems—with a strong emphasis on stability methods. They highlight how TS controllers benefit from less conservative Lyapunov- and LMI-based analyses, and point out the lack of formal stability guarantees in evolving fuzzy architectures, despite their flexibility. By contextualizing our adaptive critic neurofuzzy controller within this framework—especially given its evolving, data-adaptive nature—we align with current literature that considers stability a central challenge in fuzzy-learning controllers.

Typically, two types of critics are employed in the ACNFC: the PD critic and the fuzzy critic. While PD critics are commonly used in ACNFC frameworks, they inherently provide linear evaluations of system errors and lack the flexibility to adapt under complex nonlinear and uncertain dynamics. Fuzzy critics, by contrast, offer a richer inference mechanism that can model nonlinear error dynamics and improve learning-based adaptation. Despite this potential, to the best of our knowledge, fuzzy critics have not yet been employed within ACNFC architectures for quadrotor control. Therefore, this study aims to address this gap by designing a novel fuzzy critic for the ACNFC and evaluating its impact on quadrotor trajectory tracking performance, particularly under external disturbances. The proposed approach replaces the conventional PD critic used in [28] with a Mamdani-type fuzzy critic, and demonstrates significant improvements in accuracy, thereby advancing the capabilities of learning-based control in aerial robotics.

2 Materials and methods

2.1 Quadrotor dynamics

A quadrotor is an aircraft equipped with four rotors, each mounted on one of its four arms along with its corresponding propellers. The propellers are designed to generate upward thrust during rotation. Since opposing pairs of propellers rotate in the same direction, the drag torques produced by each pair cancel out when the rotor speeds are equal, thereby preventing the quadrotor from rotating.

To describe the dynamics of a quadrotor, two coordinate systems are employed: the body coordinate system (moving) and the inertial coordinate system (fixed). The relationship between these two coordinate systems is established using ZYX Euler angles. This means the body coordinate system is first rotated by an angle ϕ around its x-axis, then by an angle θ around the new y-axis, and finally by an angle ψ around the new z-axis to align with the inertial coordinate system. The resulting transformation is represented by a rotation matrix. This rotation matrix, which converts the body coordinate system to the inertial coordinate system, is given by equation (1). Here, c and s denote the cosine and sine functions, respectively. The Euler angles ϕ, θ, and ψ represent roll, pitch, and yaw, respectively.

$$\mathbf{R}_{\mathbf{b}}^{\mathbf{i}} = \begin{bmatrix} c_\theta c_\psi & s_\phi s_\theta c_\psi - c_\phi s_\psi & c_\phi s_\theta c_\psi + s_\phi s_\psi \\ c_\theta s_\psi & s_\phi s_\theta s_\psi + c_\phi c_\psi & c_\phi s_\theta s_\psi - s_\phi c_\psi \\ -s_\theta & s_\phi c_\theta & c_\phi c_\theta \end{bmatrix}. \tag{1}$$

This rotation matrix is used to transform vectors from the body coordinate system to the inertial coordinate system. For instance, the thrust force generated by the rotation of the propellers in the body coordinate system is represented

as $\mathbf{T^b} = \begin{bmatrix} 0 & 0 & T \end{bmatrix}^T$. To express this force in the inertial coordinate system, it can be written as:

$$\mathbf{T^i} = \mathbf{R_b^i T^b} = \begin{bmatrix} T(c_\phi s_\theta c_\psi + s_\phi s_\psi) \\ T(c_\phi s_\theta s_\psi - s_\phi c_\psi) \\ T(c_\phi c_\theta) \end{bmatrix}. \tag{2}$$

Thus, by applying Newton's second law along the three axes of the inertial coordinate system, the equations governing the translational motion of the quadrotor can be expressed as follows:

$$\begin{cases} \ddot{x} = \dfrac{T}{m}(c_\phi s_\theta c_\psi + s_\phi s_\psi) + \dfrac{f_x}{m} \\ \ddot{y} = \dfrac{T}{m}(c_\phi s_\theta s_\psi - s_\phi c_\psi) + \dfrac{f_y}{m} \\ \ddot{z} = -g + \dfrac{T}{m}(c_\phi c_\theta) + \dfrac{f_z}{m} \end{cases} \tag{3}$$

In these equations, T represents the total thrust generated by the rotation of the propellers, m is the mass of the quadrotor, and g denotes gravitational acceleration. The term $\begin{bmatrix} f_x & f_y & f_z \end{bmatrix}^T$ corresponds to the vector of external forces, including air drag, turbulence, and other environmental disturbances. The air drag forces can be modeled using the following equations:

$$\begin{cases} F_{d_x} = -\dfrac{1}{2}\rho C_d A_x V_x |V_x| \\ F_{d_y} = -\dfrac{1}{2}\rho C_d A_y V_y |V_y| \\ F_{d_z} = -\dfrac{1}{2}\rho C_d A_z V_z |V_z| \end{cases} \tag{4}$$

where ρ represents the air density, C_d is the air drag coefficient, A_i denotes the projected area of the quadrotor along the axis i, and V_i is the velocity of the quadrotor along the axis i in the inertial coordinate system.

The three equations governing the rotational motion of the quadrotor are derived by applying Euler's equations of motion around the three axes of the body coordinate system, which are expressed as follows:

$$\begin{cases} \dot{p} = \dfrac{I_y - I_z}{I_x} qr - \dfrac{J_p}{I_x}\Omega q + \dfrac{\tau_x}{I_x} + \dfrac{m_x}{I_x} \\ \dot{q} = \dfrac{I_z - I_x}{I_y} pr + \dfrac{J_p}{I_y}\Omega p + \dfrac{\tau_y}{I_y} + \dfrac{m_y}{I_y} \\ \dot{p} = \dfrac{I_x - I_y}{I_z} pq - \dfrac{J_p}{I_z}\dot{\Omega} + \dfrac{\tau_z}{I_z} + \dfrac{m_z}{I_z} \end{cases} \tag{5}$$

In these equations, $\omega^{\mathbf{b}} = \begin{bmatrix} p & q & r \end{bmatrix}^T$ represents the angular velocity vector of the quadrotor in the body coordinate system. The terms I_x, I_y, and I_z denote the moments of inertia of the quadrotor about the three principal axes in the body coordinate system, centered at the quadrotor's center of mass. The parameter J_p corresponds to the polar moment of inertia of the propellers, while Ω represents the algebraic sum of the rotational speeds of the motors. The torque vector generated by the rotation of the propellers is given by $\tau^{\mathbf{b}} = \begin{bmatrix} \tau_x & \tau_y & \tau_z \end{bmatrix}^T$, where the x and y components arise from the thrust forces of the propellers, and the z component results from the net drag torque of the rotating propellers. Additionally, $\mathbf{m^b} = \begin{bmatrix} \tau_x & \tau_y & \tau_z \end{bmatrix}^T$ represents the vector of external torques, including disturbances acting on the system.

To transform the angular velocity from the body coordinate system to the inertial coordinate system, in terms of the time derivatives of the Euler angles, the following relationship can be written:

$$\omega^{\mathbf{i}} = \mathbf{T_b^i}\omega^{\mathbf{b}};\ \mathbf{T_b^i} = \begin{bmatrix} 1 & s_\phi t_\theta & c_\phi t_\theta \\ 0 & c_\phi & -s_\phi \\ 0 & \frac{s_\phi}{c_\theta} & \frac{c_\phi}{c_\theta} \end{bmatrix}, \tag{6}$$

where $\omega^{\mathbf{i}} = \begin{bmatrix} \dot{\phi} & \dot{\theta} & \dot{\psi} \end{bmatrix}^T$ represents the angular velocity vector of the quadrotor in the inertial coordinate system, while t denotes the tangent function.

Given that the thrust force and drag torque generated by the rotation of each propeller are expressed as $T_i = b\Omega_i^2$ and $\tau_{z_i} = -sign(\Omega_i) d\Omega_i^2$, where Ω_i represents the rotational speed of the motor i, b and d are the thrust and drag

coefficient of the propellers, respectively, and considering Figure 1, along with the definition of control inputs as $U_1 = T$, $U_2 = \tau_x$, $U_3 = \tau_y$, and $U_4 = \tau_z$, the control inputs can be expressed as follows:

$$\begin{cases} U_1 = b(\Omega_1^2 + \Omega_2^2 + \Omega_3^2 + \Omega_4^2) \\ U_2 = bl(-\Omega_1^2 - \Omega_2^2 + \Omega_3^2 + \Omega_4^2) \\ U_3 = bl(\Omega_1^2 - \Omega_2^2 + \Omega_3^2 - \Omega_4^2) \\ U_4 = d(-\Omega_1^2 + \Omega_2^2 + \Omega_3^2 - \Omega_4^2) \end{cases} \tag{7}$$

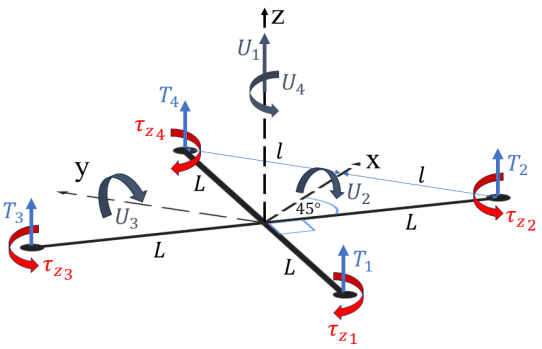

Figure 1: The quadrotor model and the propulsive forces acting on it

The model parameters analyzed in this study are presented in Table 1. These parameters were selected in accordance with the research [28] to enable a comparison with its results.

Table 1: The quadrotor model parameters

Parameter	Value	Parameter	Value
b	$2.9 \times 10^{-8}\ \frac{N.s^2}{rad^2}$	m	$40\ gr$
d	$8.8 \times 10^{-10}\ \frac{N.m.s^2}{rad^2}$	I_x	$2.093 \times 10^{-5}\ kg.m^2$
ρ	$1.2\ \frac{kg}{m^3}$	I_y	$2.093 \times 10^{-5}\ kg.m^2$
C_d	0.5	I_z	$4.122 \times 10^{-5}\ kg.m^2$
A_x	$25 \times 10^{-4}\ m^2$	l	$2\sqrt{2}\ cm$
A_y	$25 \times 10^{-4}\ m^2$	J_p	$5.036 \times 10^{-8}\ kg.m^2$
A_z	$70 \times 10^{-4}\ m^2$	Ω_{max}	$31000\ rpm$

2.2 Control

Figure 2 illustrates the control structure implemented for the quadrotor in this study. As shown in the figure, the roll and pitch degrees of freedom are controlled through the y-axis and x-axis control loops, respectively.

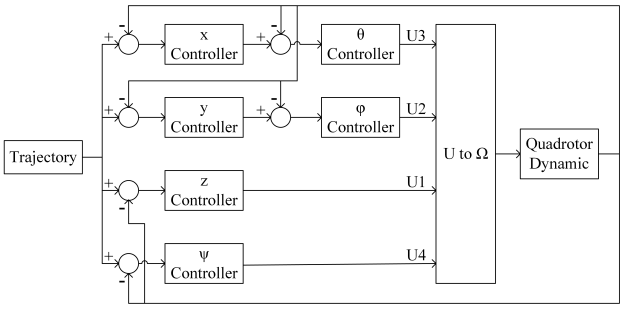

Figure 2: The control structure used for quadrotor

The overall structure of the ACNFC, comprising three main components—a neurofuzzy network, a critic agent, and a learning process—is depicted in Figure 3.

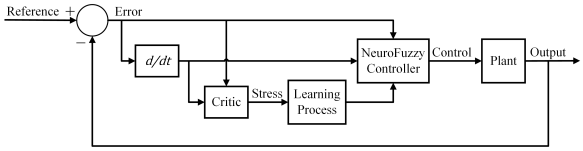

Figure 3: The structure of an ACNFC in a control loop

Neurofuzzy network: This section is based on the implementation of a Takagi-Sugeno-Kang (TSK) fuzzy logic system within a neural network framework. A schematic representation of this system, with two inputs, one output, and two membership functions (MFs) per input, is illustrated in Figure 4.

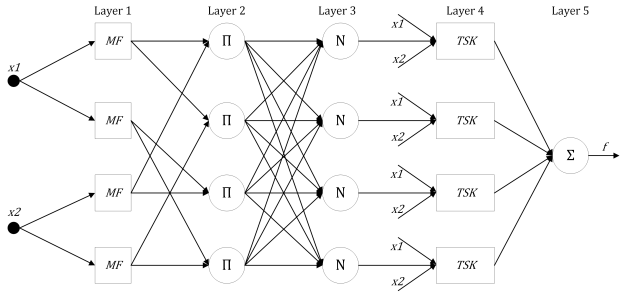

Figure 4: The schematic of a neurofuzzy network with two inputs, one output, and two MFs for each input

Fuzzification is carried out in the first layer by assigning membership degrees to the inputs based on their corresponding MFs. In other words, each node in this layer acts as a fuzzifier, mapping the inputs to their respective fuzzy sets. For two inputs, x_1 and x_2, with n and m MFs, respectively, the fuzzy sets are represented as $\mu_j(x_1)$ for $j = 1, 2, \ldots, n$ and $\mu_k(x_2)$ for $k = 1, 2, \ldots, m$. Consequently, the total number of fuzzy rules in the system is $N = n \times m$. In the second layer, the AND operation in fuzzy rules is applied. In this study, this operation is implemented by multiplying the corresponding membership values. Consequently, the output of each node in this layer can be expressed as follows:

$$u_i = \mu_j(x_1) \times \mu_k(x_2);\ i = 1, 2, ..., N, \tag{8}$$

which u_i is referred to as the activation rate of the ith rule. In the third layer, the activation rates are normalized using the following equation:

$$\bar{u}_i = \frac{u_i}{\sum_{j=1}^{N} u_j}. \tag{9}$$

The output of the fourth layer is expressed as a linear combination of the inputs of the neurofuzzy system, with the addition of a constant term, given by $a_i x_1 + b_i x_2 + c_i$. The coefficients a_i, b_i, and c_i are derived from the TSK rules

and are updated throughout the learning process. In the fifth layer, defuzzification is carried out using the following equation:

$$f = \sum_{i=1}^{N} \bar{u}_i (a_i x_1 + b_i x_2 + c_i). \tag{10}$$

In this study, the neurofuzzy network used for controlling all variables has two inputs: the controller error ($x_1 = e$) and its derivative ($x_2 = \dot{e}$). For all controllers, except for the ϕ and θ controllers with respect to the error input, three MFs are considered for each input. However, for the error input of the ϕ and θ controllers, five MFs are used. Among these MFs, the first and last are sigmoid functions, while the remaining ones are Gaussian functions. The general equations for these two functions are provided in equations (11) and (12).

$$\mu_{Sigmoid}(x) = \frac{1}{1 + e^{-\sigma(x-c)}}. \tag{11}$$

$$\mu_{Gauss}(x) = e^{-\frac{(x-c)^2}{2\sigma^2}}. \tag{12}$$

In the above equations, the shape of these two functions varies based on the parameters σ and c. The values of these parameters for all MFs are summarized in Table 2. In this table, the symbols N, NB, NS, Z, P, PB, and PS represent negative, negative big, negative small, zero, positive, positive big, and positive small, respectively. Additionally, the symbols S and G denote the sigmoid and Gaussian membership functions, respectively. Figure 5, Figure 6, and Figure 7 illustrate the MF diagrams of the neurofuzzy networks corresponding to the x and y controllers, the ϕ and θ controllers, and the ψ controller, respectively.

Table 2: The specifications of the membership functions used in the neurofuzzy networks

Controller	e				$\dot{e}$			
	MF Title	MF Type	c	σ	MF Title	MF Type	c	σ
x, y, and z	N	S	-0.5	-8	N	S	-1	-5
	Z	G	0	0.5	Z	G	0	1
	P	S	0.5	8	P	S	1	5
θ and ϕ	NB	S	$-\pi/4$	-10	N	S	$-\pi/5$	-6
	NS	G	$-3\pi/20$	$-\pi/10$				
	Z	G	0	$\pi/20$	Z	G	0	$\pi/5$
	PS	G	$3\pi/20$	$\pi/10$	P	S	$\pi/5$	6
	PB	S	$\pi/4$	10				
ψ	N	S	$-\pi/4$	-4	N	S	$-\pi/2$	-2
	Z	G	0	$\pi/4$	Z	G	0	$\pi/2$
	P	S	$\pi/4$	4	P	S	$\pi/2$	2

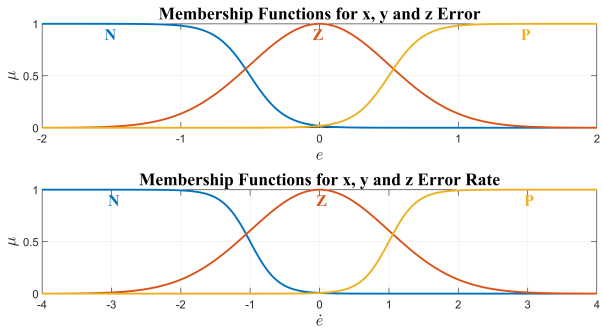

Figure 5: The membership functions of the neurofuzzy networks for the x, y, and z controllers

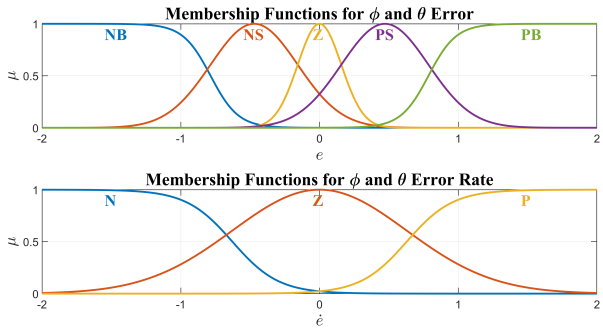

Figure 6: The membership functions of the neurofuzzy networks for the ϕ and θ controllers

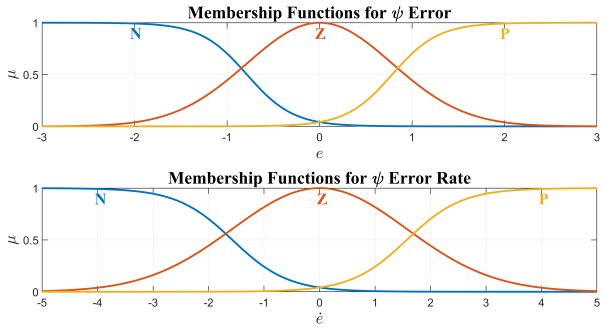

Figure 7: The membership functions of the neurofuzzy networks for the ψ controller

Critic: The role of the critic agent is to generate a reinforcement signal (r) based on the controller error and its derivative. The objective of this signal is to optimize the neurofuzzy network parameters (a_i, b_i, and c_i) through the learning process such that its value is minimized. Consequently, the cost function for this optimization problem is defined as follows:

$$E = \frac{1}{2}r^2. \tag{13}$$

As previously mentioned, two common methods are used to generate the reinforcement signal: the PD method, defined as $r = k_1 e + k_2 \dot{e}$, and the fuzzy method. The gains of the PD critics are chosen according to [28] (Table 3).

In this study, the Mamdani fuzzy logic system has been employed to design fuzzy critics. The inputs of these fuzzy systems are the controller error (e) and its derivative ($\dot{e}$), while the output is the reinforcement signal (r). Three MFs have been assigned to the inputs, and five MFs have been assigned to the output of each fuzzy critic, all of which are either sigmoid or Gaussian functions. The specifications of the MFs for the critic inputs are presented in Table 4.

Table 3: The gains of the PD critics

Controller	k_1	k_2
x and y	0.1	0.05
z	1	0.3
ϕ and θ	0.5	0.1
ψ	0.05	0.02

Likewise, the specifications of the MFs for the critic outputs are provided in Table 5. The graphical representations of these MFs are illustrated in Figure 8 to Figure 13. Since three membership functions are assigned to the inputs of the critics, each critic contains a total of nine fuzzy rules. These fuzzy rules, which are identical for all critics, are presented in Table 6. The fuzzy critics membership functions and rules were selected empirically using a trial-and-error approach, aiming to achieve accurate and reliable controller performance through iterative simulation.

Learning process: By defining w as the vector of TSK parameters and η as the learning rate, the formulation of the learning process begins with the following equation, which implies that the TSK parameters must be updated in the opposite direction to the gradient of E at a step size determined by η.

$$\Delta w = -\eta \frac{\partial E}{\partial w}. \tag{14}$$

By applying the chain rule to the derivative, equation (14) can be rewritten as follows:

$$\Delta w = -\eta \frac{\partial E}{\partial r} \times \frac{\partial r}{\partial e} \times \frac{\partial e}{\partial O} \times \frac{\partial O}{\partial f} \times \frac{\partial f}{\partial w}, \tag{15}$$

which, f represents the control effort (controller output), O is the output of the plant, $\frac{\partial O}{\partial f}$ denotes the Jacobian of the plant, and e is the controller error. Therefore,

$$e = O_{ref} - O \Rightarrow \frac{\partial e}{\partial O} = -1. \tag{16}$$

The term $\frac{\partial E}{\partial r} = r$ is derived from equation (13). Additionally, to simplify the expression, the Jacobian sign is replaced with $\frac{\partial O}{\partial f}$, and it is assumed that $\frac{\partial r}{\partial e} = 1$. As a result, the simplified form of equation (15) is given as:

$$\Delta w = \pm \eta r \frac{\partial f}{\partial w}. \tag{17}$$

In equation (17) the positive sign is applied when the Jacobian is positive, while the negative sign is used when the Jacobian is negative. The Jacobian is positive for all degrees of freedom except for the y direction, where it is negative (Figure 1). By substituting the TSK parameters for w in the above equation and considering equation (10), the update relations for the TSK parameters are obtained as follows.

$$\begin{cases} a_i := a_i \pm \eta r x_1 \bar{u}_i \\ b_i := b_i \pm \eta r x_2 \bar{u}_i \\ c_i := c_i \pm \eta r \bar{u}_i \end{cases} \tag{18}$$

Table 4: The specifications of the membership functions assigned to the inputs of fuzzy critics

Controller	e				$\dot{e}$			
	MF Title	MF Type	c	σ	MF Title	MF Type	c	σ
x	N	S	-0.5	-6	N	S	-1	-3
	Z	G	0	0.5	Z	G	0	1
	P	S	0.5	6	P	S	1	3
y	N	S	-1	-3	N	S	-1.5	-2
	Z	G	0	1	Z	G	0	1.5
	P	S	1	3	P	S	1.5	2
z	N	S	-0.25	-12	N	S	-0.25	-12
	Z	G	0	0.25	Z	G	0	0.25
	P	S	0.25	12	P	S	0.25	12
ϕ	N	S	-2.5	-1.2	N	S	-5	-0.6
	Z	G	0	2.5	Z	G	0	5
	P	S	2.5	1.2	P	S	5	0.6
θ	N	S	-2	-1.5	N	S	-4	-0.75
	Z	G	0	2	Z	G	0	4
	P	S	2	1.5	P	S	4	0.75
ψ	N	S	-0.05	-60	N	S	-0.5	-6
	Z	G	0	0.05	Z	G	0	0.5
	P	S	0.05	60	P	S	0.5	6

Table 5: The specifications of the membership functions assigned to the output of fuzzy critics

Controller	r			
	MF Title	MF Type	c	σ
x, y, z, ϕ, and θ	NB	S	-0.45	-20
	NS	G	-0.3	0.15
	Z	G	0	0.15
	PS	G	0.3	0.15
	PB	S	0.45	20
ψ	NB	S	-0.1	-90
	NS	G	$-2/30$	$1/30$
	Z	G	0	$1/30$
	PS	G	$2/30$	$1/30$
	PB	S	0.1	90

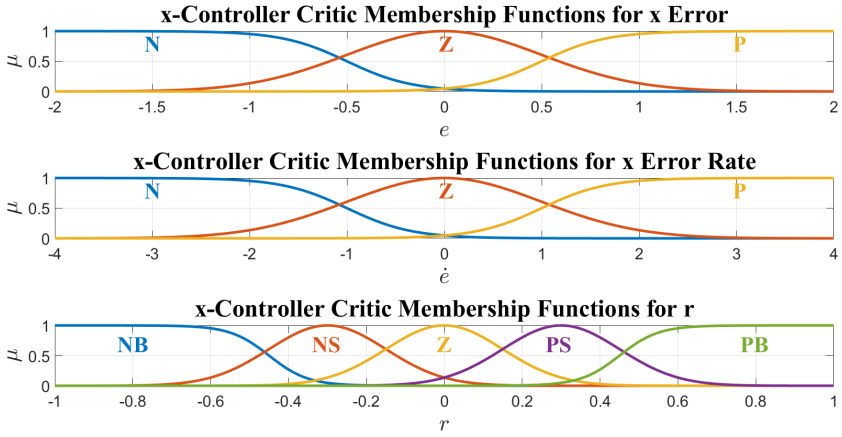

Figure 8: The membership functions of the x controller fuzzy critic

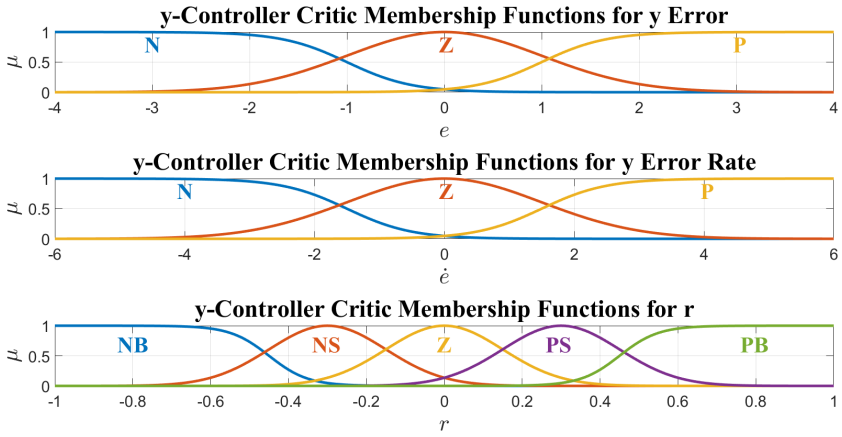

Figure 9: The membership functions of the y controller fuzzy critic

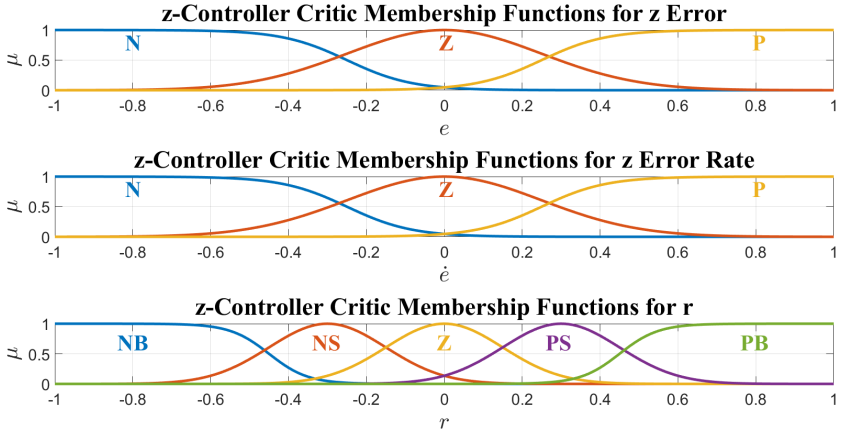

Figure 10: The membership functions of the z controller fuzzy critic

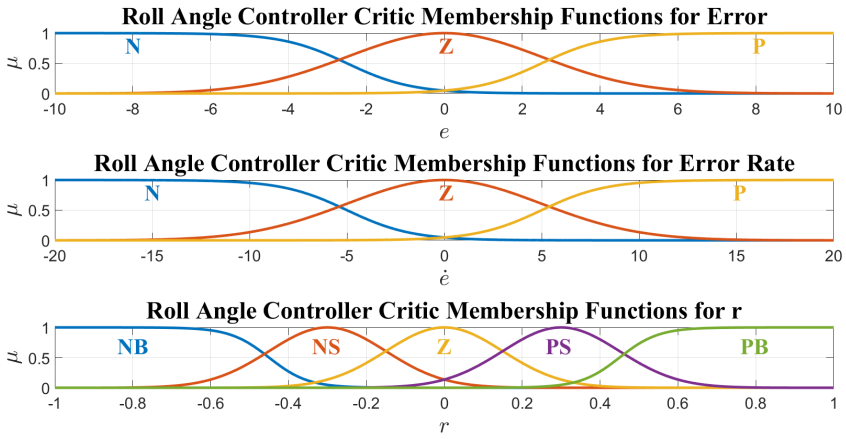

Figure 11: The membership functions of the ϕ controller fuzzy critic

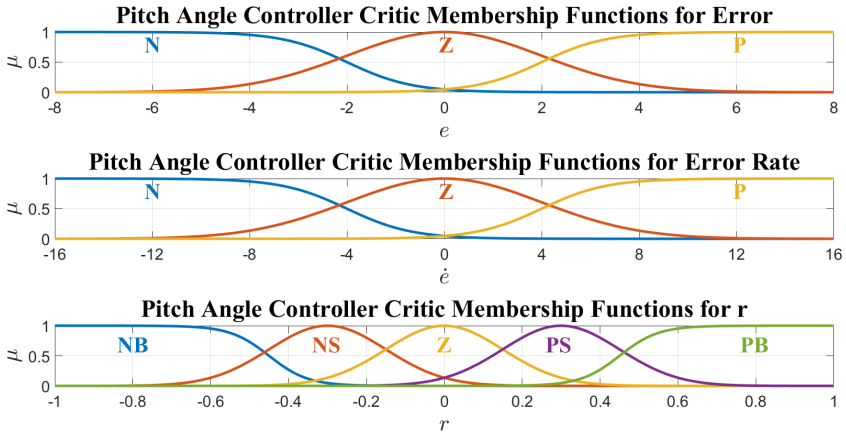

Figure 12: The membership functions of the θ controller fuzzy critic

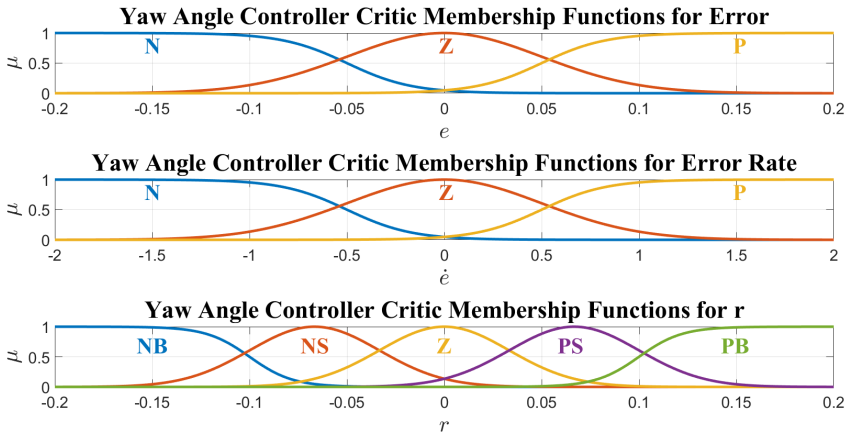

Figure 13: The membership functions of the ψ controller fuzzy critic

Table 6: Fuzzy rules of the fuzzy critics

e \ $\dot{e}$	N	Z	P
N	NB	NS	Z
Z	NS	Z	PS
P	Z	PS	PB

The learning rates assigned to the controllers are presented in Table 7, and are defined based on the findings of [28]. Notably, for the controllers corresponding to x and y, the learning rate is set to 0.1 during the first 10 seconds. Between 10 and 20 seconds, this rate increases to 0.25, and from the 20th second onward, it is further increased to 1.

Table 7: The learning rates assigned to the controllers

Controller	Learning rate (η)		
	$t < 10$	$10 \leq t < 20$	$t \geq 20$
x and y	0.1	0.25	1
z	0.5		
ϕ and θ	0.005		
ψ	0.05		

3 Results and discussion

To evaluate the performance of the ACNFC with fuzzy critics in quadrotor control and compare it with the ACNFC utilizing PD critics, simulations were conducted in the Simulink environment of MATLAB R2021b with fixed step size of 0.01 seconds. The simulation is configured such that a spiral trajectory is defined as the desired path for the quadrotor, and the accuracy of the controllers in tracking this path is assessed. The performance evaluation in this study is based on the root mean square error (RMSE), which is calculated using the following equation:

$$RMSE = \sqrt{\frac{1}{N}\sum_{i=1}^{N}(x_i - x_{d,i})^2}. \tag{19}$$

which x_i represents the i-th component of the signal being evaluated, $x_{d,i}$ is its desired value, and N denotes the total number of components. The desired trajectory defined in this study follows the same pattern as in [28] and is expressed as a function of time in equation (20). The corresponding diagram is illustrated in Figure 14.

$$\begin{cases} x_d = 10(cos(0.5t) - 1) \\ y_d = 10sin(0.5t) \\ z_d = t \end{cases} \tag{20}$$

Table 8 presents the tracking errors of the ACNFCs with PD and fuzzy critics for the desired values of x, y, and z. Additionally, the graphs illustrating the tracking performance of these controllers are shown in figures 15 to 17. According to Table 8, although the fuzzy critic improved trajectory tracking in the horizontal directions (x and y), an increase of 11.25% in the z-axis RMSE (height tracking error) was observed compared to the PD critic. This rise can be attributed to several interconnected factors. First, the vertical motion of the quadrotor is highly sensitive to variations in thrust force due to its direct opposition to gravity. Small inconsistencies in the output of the fuzzy critic-especially during rapid vertical changes-can lead to amplified deviations in altitude. Another contributing factor is the smoother behavior of PD critics in low-error regimes, which may have provided slightly better fine control for maintaining altitude.

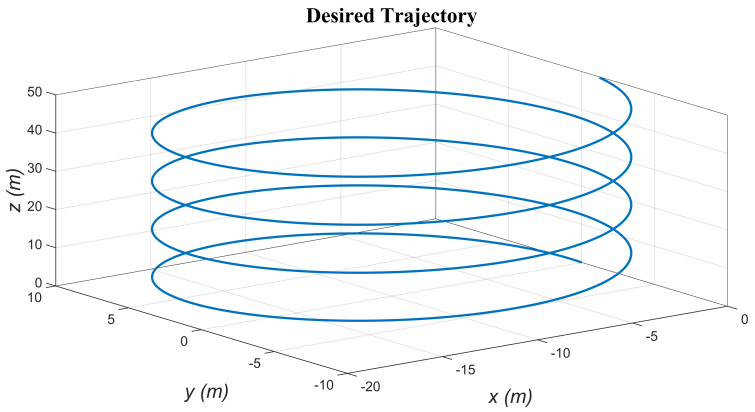

Figure 14: The desired trajectory

Table 8: The tracking error of the two ACNFCs, one utilizing PD critics and the other employing fuzzy critics

Critic Type	x-RMSE	y-RMSE	z-RMSE
PD	0.0974 m	0.1573 m	0.0024 m
Fuzzy	0.0287 m	0.0948 m	0.0026 m
Change	-70.59%	-39.78%	11.25%

To evaluate the performance of the ACNFC with the newly designed fuzzy critic under external disturbances, a disturbance in the form of white noise (Figure 18) was applied as an external moment about the x-axis of the quadrotor model (m_x). Table 9 presents the tracking errors of the ACNFCs with PD and fuzzy critics for the desired values of x, y, and z in the presence of disturbance. The simulation graphs are presented in figures 19 through 21.

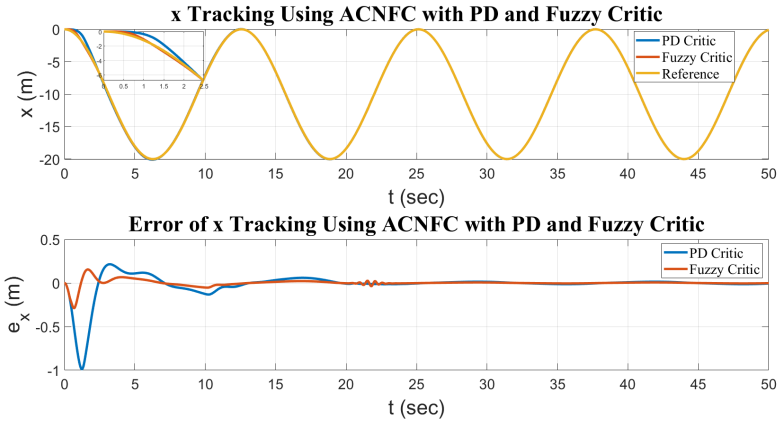

Figure 15: Plot of x tracking (top) and its error (bottom) using ACNFCs with PD and fuzzy critics

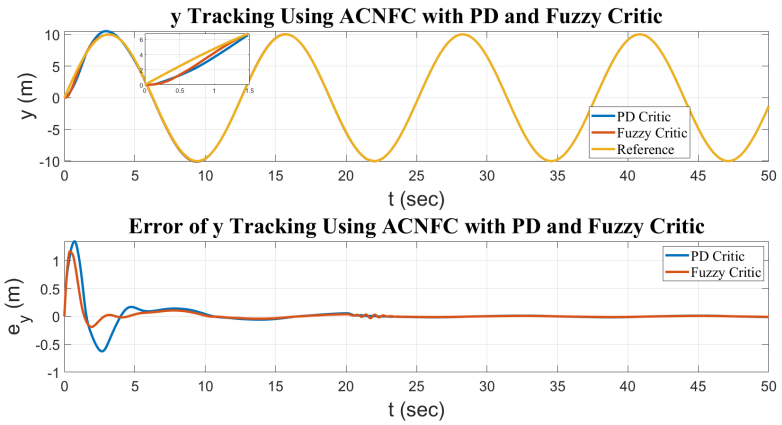

Figure 16: Plot of y tracking (top) and its error (bottom) using ACNFCs with PD and fuzzy critics

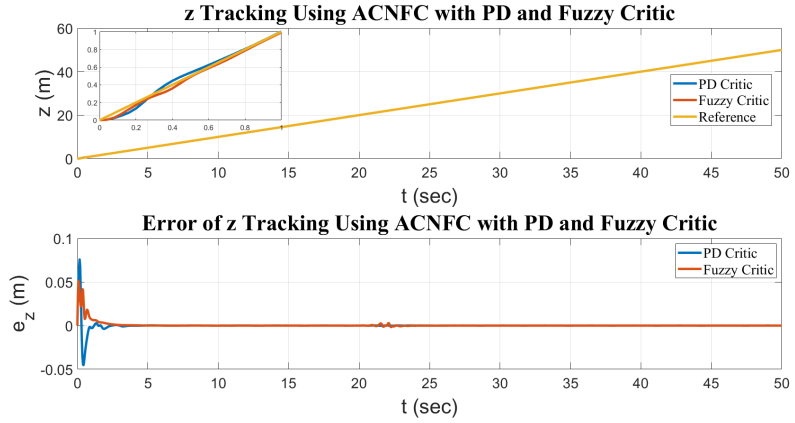

Figure 17: Plot of z tracking (top) and its error (bottom) using ACNFCs with PD and fuzzy critics

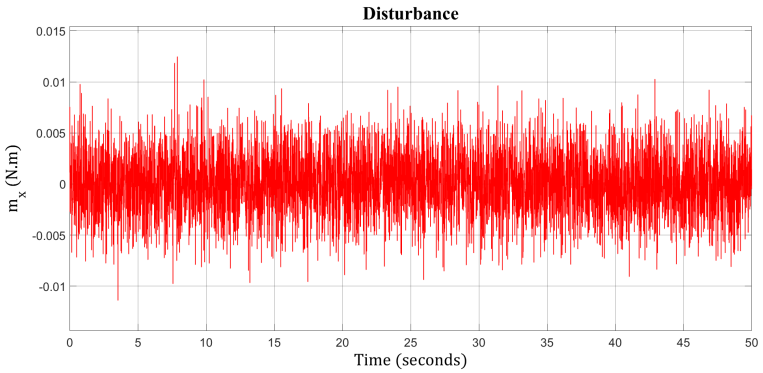

Figure 18: The disturbance applied to the quadrotor model as an external moment about the x-axis (m_x)

Table 9: The tracking error of the two ACNFCs, one utilizing PD critics and the other employing fuzzy critics in the presence of disturbance

Critic Type	x-RMSE	y-RMSE	z-RMSE
PD	0.0980 m	0.1540 m	0.0023 m
Fuzzy	0.0274 m	0.1358 m	0.0025 m
Change	-72.01%	-11.82%	7.71%

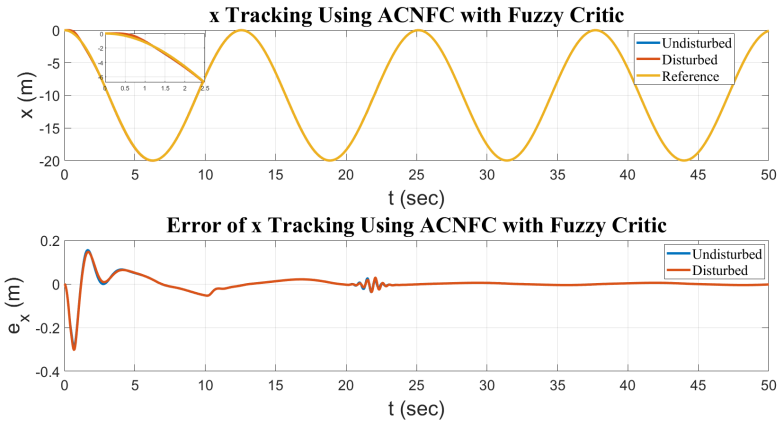

Figure 19: Plot of x tracking and its error using the ACNFC with fuzzy critics in the presence and absence of disturbance

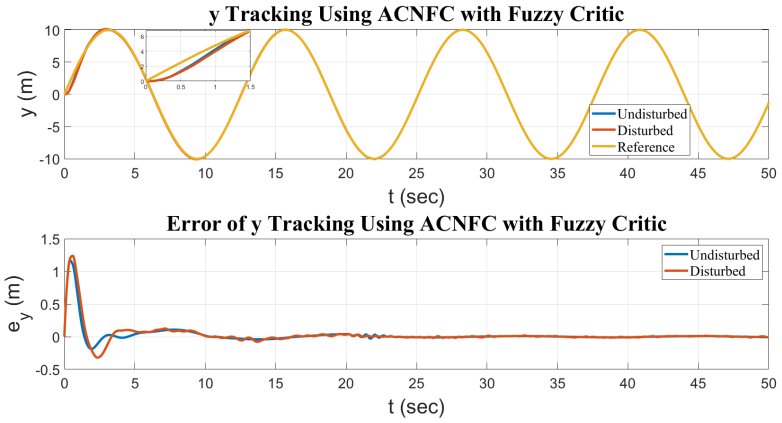

Figure 20: Plot of y tracking and its error using the ACNFC with fuzzy critics in the presence and absence of disturbance

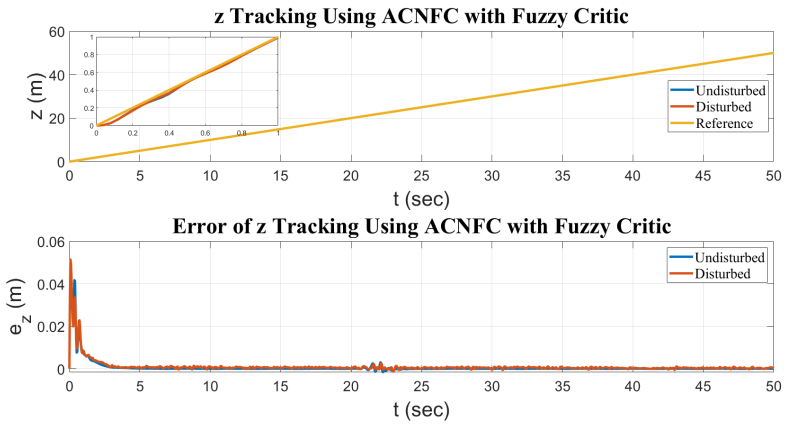

Figure 21: Plot of z tracking and its error using the ACNFC with fuzzy critics in the presence and absence of disturbance

To facilitate a comprehensive performance comparison, Table 10 consolidates the RMSE values of the ACNFC under both nominal and disturbed conditions for PD and fuzzy critics.

Table 10: Summary of RMSE performance for ACNFCs under nominal and disturbed conditions

Condition	Nominal			Disturbed		
RMSE (m)	x-RMSE	y-RMSE	z-RMSE	x-RMSE	y-RMSE	z-RMSE
PD Critic	0.0974	0.1573	0.0024	0.0980	0.1540	0.0023
Fuzzy Critic	0.0287	0.0948	0.0026	0.0274	0.1358	0.0025
Change (%)	−70.59	−39.78	11.25	−72.01	−11.82	7.71

4 Conclusion

This study aimed to enhance the performance of an ACNFC in tracking a spiral path by designing a fuzzy critic and replacing the PD critic with a fuzzy one.

As shown in Table 8, it can be concluded that replacing the PD critic with a fuzzy critic improved the ACNFC's performance in tracking the x and y of the trajectory by 70.59% and 39.78%, respectively. However, it resulted in an 11.25% increase in the height tracking error. Despite this increase in height error, the controller still demonstrated a relatively low error rate in height tracking. Therefore, it can be concluded that changing the critic type from PD to fuzzy improved the overall performance of the controller in following the path. This conclusion is further supported by the graphs presented in figures 15 through 17.

Next, to evaluate the performance of the ACNFC with a fuzzy critic in the presence of external disturbances, white noise was introduced as an external disturbance into the system. The results demonstrate the controller's effective performance in trajectory tracking even in the presence of this disturbance and in mitigating its effects. This is further illustrated by the graphs in figures 19 through 21.

This improvement in performance is accompanied by an increase in computational complexity. The added complexity primarily stems from the inherent structure of the Mamdani fuzzy logic system, which involves the use of multiple membership functions and the formulation of fuzzy inference rules that are customized for each critic.

4.1 Limitations and future work

Despite the performance improvements demonstrated by the proposed ACNFC with fuzzy critics, several limitations remain in the current methodology. First, the study compares the fuzzy critic only against a PD critic within the ACNFC

framework, without benchmarking against other advanced control strategies such as Model Predictive Control (MPC) or Reinforcement Learning (RL). This narrow comparison limits the generalizability of the performance claims. Second, all experiments were conducted in a simulation environment, and no hardware-in-the-loop or real-world flight tests were performed. As a result, the controller's robustness to real-world uncertainties such as sensor noise, communication delays, or actuator saturation remains unverified. Third, the fuzzy critic's design—including the choice of membership functions, rules, and parameters—is based on expert knowledge and heuristics rather than a systematic optimization process. While effective in this case, such hand-crafted tuning may not generalize to more complex or dynamic flight scenarios.

To address these limitations, future work may explore integrating more sophisticated control paradigms. RL offers a promising direction by enabling the automatic learning of control policies through interaction with the environment. Unlike fuzzy systems that rely on predefined rules, RL can discover optimal policies even in high-dimensional and stochastic settings. Moreover, RL can inherently learn from disturbance-rich environments, potentially improving generalization and robustness. However, RL-based controllers often lack interpretability and require significant computational resources for training, which may pose challenges for deployment.

MPC, on the other hand, provides a model-based framework that optimizes control actions over a prediction horizon while enforcing system constraints. MPC is particularly effective at handling multi-variable systems and state/input constraints, and could offer better performance guarantees in structured environments. Additionally, MPC naturally incorporates disturbance rejection and trajectory tracking into its optimization. Nevertheless, MPC's reliance on accurate system models and its computational complexity may limit real-time applicability, especially in highly dynamic or uncertain conditions. Therefore, hybrid approaches-such as fuzzy-tuned MPC or RL-enhanced ACNFC-could be explored in future studies to combine the adaptability of learning-based methods with the predictability of model-based control.

Acknowledgement

The authors wish to express their appreciation for several excellent suggestions for improvements in this paper made by the referees.

References

[1] D. Allahverdy, A. Fakharian, M. B. Menhaj, *Back-stepping integral sliding mode control with iterative learning control algorithm for quadrotor UAVs*, Journal of Electrical Engineering and Technology, **14** (2019), 2539-2547. https://doi.org/10.1007/s42835-019-00257-z

[2] M. E. Antonio-Toledo, E. N. Sanchez, A. Y. Alanis, J. Flórez, M. A. Perez-Cisneros, *Real-time integral backstepping with sliding mode control for a quadrotor UAV*, IFAC-PapersOnLine, **51**(13) (2018), 549-554. https://doi.org/10.1016/j.ifacol.2018.07.337

[3] A. Bahari Kordabad, M. Boroushaki, *Emotional learning based intelligent controller for mimo peripheral milling process*, Journal of Applied and Computational Mechanics, **6**(3) (2020), 480-492. https://doi.org/10.22055/JACM.2019.30188.1696

[4] S. Bouabdallah, R. Siegwart, *Design and control of a miniature quadrotor*, In Advances in Unmanned Aerial Vehicles: State of the Art and the Road to Autonomy, Dordrecht: Springer Netherlands, (2007), 171-210. https://doi.org/10.1007/978-1-4020-6114-1_6

[5] W. Budiharto, E. Irwansyah, J. S. Suroso, A. Chowanda, H. Ngarianto, A. A. S. Gunawan, *Mapping and 3D modelling using quadrotor drone and GIS software*, Journal of Big Data, **8** (2021), 1-12. https://doi.org/10.1186/s40537-021-00436-8

[6] A. S. Elkhatem, S. N. Engin, *Robust LQR and LQR-PI control strategies based on adaptive weighting matrix selection for a UAV position and attitude tracking control*, Alexandria Engineering Journal, **61**(8) (2022), 6275-6292. https://doi.org/10.1016/j.aej.2021.11.057

[7] R. L. Finn, D. Wright, *Unmanned aircraft systems: Surveillance, ethics and privacy in civil applications*, Computer Law and Security Review, **28**(2) (2012), 184-194. https://doi.org/10.1016/j.clsr.2012.01.005

[8] C. Fu, A. Sarabakha, E. Kayacan, C. Wagner, R. John, J. M. Garibaldi, *Input uncertainty sensitivity enhanced nonsingleton fuzzy logic controllers for long-term navigation of quadrotor UAVs*, IEEE/ASME Transactions on Mechatronics, **23**(2) (2018), 725-734. https://doi.org/10.1109/TMECH.2018.2810947

[9] H. Hassani, A. Mansouri, A. Ahaitouf, *Control system of a quadrotor UAV with an optimized backstepping controller*, 2019 International Conference on Intelligent Systems and Advanced Computing Sciences (ISACS), IEEE, (2019), 1-7. https://doi.org/10.1109/ISACS48493.2019.9068874

[10] A. Hentout, A. Maoudj, A. Kouider, *Shortest path planning and efficient fuzzy logic control of mobile robots in indoor static and dynamic environments*, Romanian Journal of Information Science and Technology, **27**(94) (2024), 21-36. https://doi.org/10.59277/ROMJIST.2024.94.02

[11] M. Jafari, A. M. Shahri, S. B. Shouraki, *Attitude control of a quadrotor using brain emotional learning based intelligent controller*, 2013 13th Iranian Conference on Fuzzy Systems (IFSC), IEEE, (2013), 1-5. https://doi.org/10.1109/IFSC.2013.6675672

[12] H. Jayakrishnan, *Position and attitude control of a quadrotor UAV using super twisting sliding mode*, IFAC-PapersOnLine, **49**(1) (2016), 284-289. https://doi.org/10.1016/j.ifacol.2016.03.067

[13] E. Joelianto, D. Christian, A. Samsi, *Swarm control of an unmanned quadrotor model with LQR weighting matrix optimization using genetic algorithm*, Journal of Mechatronics, Electrical Power, and Vehicular Technology, **11**(1) (2020), 1-10. https://dx.doi.org/10.14203/j.mev.2020.v11.1-10

[14] M. Labbadi, M. Cherkaoui, *Robust adaptive backstepping fast terminal sliding mode controller for uncertain quadrotor UAV*, Aerospace Science and Technology, **93** (2019), 105306. https://doi.org/10.1016/j.ast.2019.105306

[15] D. Lara Alabazares, A. Rabhi, C. Pegard, F. Torres Garcia, G. Romero Galvan, *Quadrotor UAV attitude stabilization using fuzzy robust control*, Transactions of the Institute of Measurement and Control, **43**(12) (2021), 2599-2614. https://doi.org/10.1177/01423312211002588

[16] J. Liu, W. Gai, J. Zhang, Y. Li, *Nonlinear adaptive backstepping with ESO for the quadrotor trajectory tracking control in the multiple disturbances*, International Journal of Control, Automation and Systems, **17** (2019), 2754-2768. https://doi.org/10.1007/s12555-018-0909-9

[17] I. Lopez-Sanchez, J. Moreno-Valenzuela, *PID control of quadrotor UAVs: A survey*, Annual Reviews in Control, **56** (2023), 100900. https://doi.org/10.1016/j.arcontrol.2023.100900

[18] O. Mehrabi, A. Fakharian, M. Siahi, A. Ramezani, *Fuzzy radial basis function least square policy iteration: A novel critic-only reinforcement learning framework*, Iranian Journal of Fuzzy Systems, **22**(2) (2025), 59-80. https://doi.org/10.22111/ijfs.2025.48345.8503

[19] J. Moreno-Valenzuela, R. Pérez-Alcocer, M. Guerrero-Medina, A. Dzul, *Nonlinear PID-type controller for quadrotor trajectory tracking*, IEEE/ASME Transactions on Mechatronics, **23**(5) (2018), 2436-2447. https://doi.org/10.1109/TMECH.2018.2855161

[20] Z. Mustapa, S. Saat, S. Husin, N. Abas, *Altitude controller design for multi-copter UAV*, 2014 International Conference on Computer, Communications, and Control Technology (I4CT), IEEE, (2014), 382-387. https://doi.org/10.1109/I4CT.2014.6914210

[21] E. Okyere, A. Bousbaine, G. T. Poyi, A. K. Joseph, J. M. Andrade, *LQR controller design for quad-rotor helicopters*, The Journal of Engineering, **2019**(17) (2019), 4003-4007. https://doi.org/10.1049/joe.2018.8126

[22] J. Pan, B. Shao, J. Xiong, Q. Zhang, *Attitude control of quadrotor UAVs based on adaptive sliding mode*, International Journal of Control, Automation and Systems, **21**(8) (2023), 2698-2707. https://doi.org/10.1007/s12555-022-0189-2

[23] R. E. Precup, A. T. Nguyen, S. Blažič, *A survey on fuzzy control for mechatronics applications*, International Journal of Systems Science, **55**(4) (2024), 771-813. https://doi.org/10.1080/00207721.2023.2293486

[24] S. Preitl, R. E. Precup, F. János, B. Bede, *Iterative feedback tuning in fuzzy control systems. Theory and applications*, Acta Polytechnica Hungarica, **3**(3) (2006). https://acta.uni-obuda.hu/Preitl_Precup_Fodor_Bede_7.pdf

[25] M. Rabah, A. Rohan, Y. J. Han, S. H. Kim, *Design of fuzzy-PID controller for quadcopter trajectory-tracking*, International Journal of Fuzzy Logic and Intelligent Systems, **18**(3) (2018), 204-213. https://doi.org/10.5391/IJFIS.2018.18.3.204

[26] S. Radiansyah, M. Kusrini, L. Prasetyo, *Quadcopter applications for wildlife monitoring*, IOP Conference Series: Earth and Environmental Science, IOP Publishing, **54**(1) (2017), 012066. https://doi.org/10.1088/1755-1315/54/1/012066

[27] M. F. Rahmat, A. Eltayeb, M. A. M. Basri, *Adaptive feedback linearization controller for stabilization of quadrotor UAV*, International Journal of Integrated Engineering, **12**(4) (2020), 1-17. https://doi.org/10.30880/ijie.2020.12.04.001

[28] M. S. Ramezani, S. Ajami, H. Ghafarirad, *Path-tracking control of quadrotor using adaptive critic-based neurofuzzy controller*, 2021 9th RSI International Conference on Robotics and Mechatronics (ICRoM), IEEE, (2021), 248-254. https://doi.org/10.1109/ICRoM54204.2021.9663523

[29] H. Razmi, S. Afshinfar, *Neural network-based adaptive sliding mode control design for position and attitude control of a quadrotor UAV*, Aerospace Science and Technology, **91** (2019), 12-27. https://doi.org/10.1016/j.ast.2019.04.055

[30] E. X. Rodriguez, Q. Lu, *Tuning PID controller for quadrotor using particle swarm optimization*, 2024 21st International Conference on Ubiquitous Robots (UR), IEEE, (2024), 168-175. https://doi.org/10.1109/UR61395.2024.10597517

[31] Y. J. Ryoo, *An autonomous control of fuzzy-PD controller for quadcopter*, International Journal of Fuzzy Logic and Intelligent Systems, **17**(2) (2017), 107-113. https://doi.org/10.5391/IJFIS.2017.17.2.107

[32] D. Severtson, N. Callow, K. Flower, A. Neuhaus, M. Olejnik, C. Nansen, *Unmanned aerial vehicle canopy reflectance data detects potassium deficiency and green peach aphid susceptibility in canola*, Precision Agriculture, **17** (2016), 659-677. https://doi.org/10.1007/s11119-016-9442-0

[33] A. Shafiekhani, M. J. Mahjoob, M. Akraminia, *Design and implementation of an adaptive critic-based neuro-fuzzy controller on an unmanned bicycle*, Mechatronics, **28** (2015), 115-123. https://doi.org/10.1016/j.mechatronics.2015.04.010

[34] A. Sunay, A. Altan, E. Belge, R. Hacioğlu, *Investigation of route tracking performance with adaptive PID controller in quadrotor*, European Journal of Technique (EJT), **10**(1) (2020), 160-172. https://doi.org/10.36222/ejt.652828

[35] D. C. Tosun, Y. Işık, H. Korul, *Comparison of PID and LQR controllers on a quadrotor helicopter*, International Journal of Systems Applications, Engineering and Development, **9** (2015), 136-143. https://api.semanticscholar.org/CorpusID:174789345

[36] R. Vatankhah, M. Rahaeifard, A. Alasty, *Vibration control of vehicle suspension system using adaptive critic-based neurofuzzy controller*, 2009 6th International Symposium on Mechatronics and its Applications, IEEE, (2009), 1-6. https://doi.org/10.1109/ISMA.2009.5164809

[37] J. Wen, F. Wang, *Stable levitation of single-point levitation systems for Maglev trains by improved cascade control*, Romanian Journal of Information Science and Technology, **27** (2024), 348-361. https://doi.org/10.59277/ROMJIST.2024.3-4.08